# Comprehensive Analysis of Small-Signal Parameters of Fully Strained and Partially Relaxed High Al-Content Lattice Mismatched $Al_mGa_{1-m}N$/GaN HEMTs

Rashmi, Abhinav Kranti, Subhasis Haldar, Mridula Gupta, *Member, IEEE*, and R. S. Gupta, *Senior Member, IEEE*

***Abstract*—This paper proposes an accurate model to investigate the small-signal microwave parameters of fully strained (FS) and partially relaxed (PR) $Al_mGa_{1-m}N$/GaN high electron-mobility transistors (HEMTs). It is observed that elastic strain relaxation of the $Al_mGa_{1-m}N$ layer imposes an upper limit on the maximum two-dimensional electron-gas sheet charge density and is, thus, extremely critical in determining the microwave performance of high Al-content $Al_mGa_{1-m}N$/GaN HEMTs. The model incorporates the effects of strain relaxation of the barrier layer, field-dependent mobility, parasitic source/drain resistance, and velocity saturation to evaluate drain current, transconductance, drain conductance, cutoff frequency, and transit time of FS and PR $Al_mGa_{1-m}N$/GaN HEMTs with different Al mole fractions. The proposed model predicts a high drain current of 5.94 A/mm for a PR 0.3-$\mu$m $Al_{0.4}Ga_{0.6}N$/GaN HEMT, which is in close proximity with previously published simulated results. A peak transconductance of 154 mS/mm is also estimated for a 1-$\mu$m gate-length device with aluminum concentration of 15% (FS), which is in close agreement with previously published measured data. A high cutoff frequency of 21.09 GHz was predicted for a 0.6-$\mu$m device with an Al mole fraction of 0.5 (PR), thus showing the potential of AlGaN/GaN HEMTs for microwave applications.**

***Index Terms*—$Al_mGa_{1-m}N$/GaN HEMTs, current–voltage characteristics, cutoff frequency, drain conductance, strain relaxation, threshold voltage, transconductance, transit time.**

## I. Introduction

HIGH electron-mobility transistors (HEMTs) have shown promising performance in very high-speed integrated circuits owing to their very high switching speed and low power consumption. Over the past few years, AlGaN/GaN HEMTs have emerged strongly as attractive candidates for high-power high-temperature high-speed applications at frequencies well into the microwave region [1]–[8]. The presence of strong spontaneous and strain-induced piezoelectric polarization fields due to lattice mismatch between AlGaN and GaN layers, in addition to the large bandgap energy, high saturation velocity, large breakdown field, large conduction-band discontinuity, and high thermal stability [9]–[11] are some of the characteristic features of the AlGaN/GaN material system that lead to outstanding performance of GaN-based HEMTs [12]–[18].

The key to enhanced performance of HEMTs is improved charge confinement and superior carrier transport that result from a very high two-dimensional electron gas (2-DEG) sheet charge density ($n_s$) with concomitant high mobility. The conduction-band discontinuity between the AlGaN barrier and GaN channel layers and the doping density of AlGaN are the two most important parameters that can be tailored so as to attain high $n_s$. The upper limit on doping density is, however, imposed by the requirement of the nonleaky Schottky barrier and by electron traps in the barrier that reduce the conduction ability of the 2-DEG. Thus, increasing the conduction-band offset seems to be the best option to improve HEMT performance. Furthermore, 2-DEG density in AlGaN/GaN HEMTs is predominantly determined by the piezoelectric and spontaneous polarization, which, in turn, is controlled by the alloy composition (Al content) of the $Al_mGa_{1-m}N$ barrier [19]–[22]. Piezoelectric polarization of AlGaN on GaN is also determined by the elastic strain in AlGaN, resulting from the lattice mismatch between AlGaN and GaN layers [23]–[25]. Thus, any factor that affects the strain in the AlGaN layer would be critical in determining the polarization charges.

An increase in the Al-content/mole fraction ($m$) of $Al_mGa_{1-m}N$ barrier was proposed to yield improved charge confinement, larger 2-DEG density-mobility ($n_s - \mu$) product, reduced hot carrier injection from GaN to AlGaN, and higher breakdown field through increased bandgap, larger conduction-band discontinuity, higher Schottky barrier height, and stronger polarization effects [4], [26]–[28]. A higher Schottky barrier also leads to more stable gate–metal/AlGaN interface at elevated temperatures, thus predicting higher equivalent figures-of-merit with Al-rich devices. Zhang and Singh [29] have shown that, as the Al composition increases, the 2-DEG density increases and electrons are pushed more closely to the interface, improving the carrier confinement. However, this makes the interface roughness effects more serious, leading

Manuscript received February 12, 2002. This work was supported by the University Grants Commission, by the Government of India, and by the Council for Scientific and Industrial Research.

Rashmi, M. Gupta, and R. S. Gupta are with the Semiconductor Devices Research Laboratory, Department of Electronic Science, University of Delhi, New Delhi 110 021, India (e-mail: rsgu@bol.net.in).

A. Kranti was with the Semiconductor Devices Research Laboratory, Department of Electronic Science, University of Delhi, New Delhi 110 021, India. He is now with the Electromagnetic Microwave and Communications Laboratory, Université Catholique de Louvain, B-1348 Louvain-la-Neuve, Belgium.

S. Haldar is with the Department of Physics, Motilal Nehru College, University of Delhi, New Delhi 110 021, India.

Digital Object Identifier 10.1109/TMTT.2002.807678

to a larger scattering rate. Also, the device becomes more difficult to turn on. Further, increase in Al content also leads to increased lattice mismatch between AlGaN and GaN, which can no longer be accommodated completely by internal strains, thus leading to the formation of misfit dislocations or grains [21], [24]. Under such conditions, the barrier layer is said to be relaxed of its elastic strain, consequently reducing the strain-induced piezoelectric polarization charge density [30]–[33]. These effects result in the degradation of device performance and, therefore, there has to be an optimization in the Al content. The Al content in $Al_mGa_{1-m}N$ should be as high as possible, consistent with obtaining low ionization energies for donors, good ohmic contacts, and minimum traps. The defect states arising from dislocations and surface states act as electron traps that limit the microwave performance of the device. The various trapping effects can be minimized through improvements in material growth and process technology for AlGaN/GaN material system [11], [21]. A well-processed device with reduced traps is the key to improved performance, more so in the high Al-content devices.

Although significant progress has been made over the past few years, additional development work in terms of modeling of small-signal parameters is required for GaN-based HEMTs, especially for the high Al-content structures to aid in technology development, device structure optimization, and advanced design. Research efforts thus far in $Al_mGa_{1-m}N$/GaN HEMTs have focused on transport phenomena and charge control in fully strained (FS) devices [29], [34]–[41]. Investigations in high Al-content HEMTs have been directed toward analyzing the effect of relaxation on 2-DEG density and mobility to estimate the critical thickness for relaxation [14], [31]–[33]. No models are yet available to study the impact of strain relaxation on $I$–$V$ characteristics and small-signal parameters of AlGaN/GaN HEMTs, which are extremely important for evaluating microwave performance of the device.

This paper proposes an accurate model for current–voltage characteristics and small-signal microwave parameters, namely, drain conductance, transconductance, cutoff frequency, and transit time of FS and partially relaxed (PR) $Al_mGa_{1-m}N$/GaN HEMTs, incorporating the effects of spontaneous and strain-dependent piezoelectric polarization fields. The effects of important technological parameters such as aluminum concentration, gate length, barrier thickness, and doping of the $Al_mGa_{1-m}N$ layer on device characteristics have been analyzed in detail. The model has been verified with published experimental/simulated data wherever available. The authors were not able to compare some of their predicted results with experimental/simulated data due to the nonavailability of published results. This current model does not include the effects of electron traps, surface states, and dislocations, which act to limit the microwave performance of $Al_mGa_{1-m}N$/GaN HEMTs. A model accounting for the various trapping phenomena would be valuable, but is beyond the scope of this paper. However, the model in its current form would still be useful for performance prediction and device structure optimization, which are extremely important for assessing the microwave performance of FS, PR, and fully relaxed $Al_mGa_{1-m}N$/GaN heterostructures.

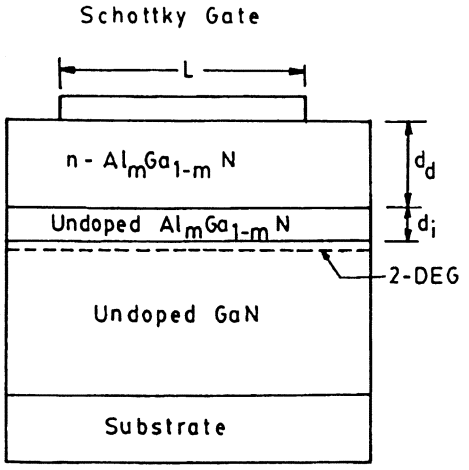


Fig. 1. Schematic diagram of the $Al_mGa_{1-m}N$/GaN HEMT with doped barrier thickness ($d_d$) and spacer layer thickness ($d_i$).

## II. Theoretical Considerations

The basic charge-control equation for 2-DEG sheet charge density formed at the $Al_mGa_{1-m}N$/GaN heterointerface (Fig. 1) is obtained [36] as

$$n_s(m,x) = \frac{\varepsilon(m)}{q\cdot(d_d+d_i+\Delta d)}\left(V_{\rm gs}-V_c(x)-V_{\rm th}(m)\right) \tag{1}$$

where $q$ is the electron charge, $m$ is the Al mole fraction in $Al_mGa_{1-m}N$, $\varepsilon(m)$ is the AlGaN dielectric constant, $d_d$ is the AlGaN barrier thickness, $d_i$ is the spacer layer thickness, $\Delta d$ is the effective thickness of 2-DEG, $V_{\rm gs}$ is the applied gate–source voltage, and $V_c(x)$ is the channel potential at $x$. The threshold voltage $V_{\rm th}(m)$ of the AlGaN/GaN HEMT is strongly dependent on polarization charge density and is obtained as

$$V_{\rm th}(m) = \phi_m(m) - \Delta E_c(m) - \frac{qN_d d_d^2}{2\varepsilon(m)} - \frac{\sigma(m)}{\varepsilon(m)}(d) \tag{2}$$

where $\phi_m(m)$ is the Schottky barrier height, $\Delta E_c(m)$ is the conduction-band discontinuity, $N_d$ is the doping density of the AlGaN barrier, $d = d_d + d_i$, and $\sigma(m)$ is the net polarization induced sheet charge density at the $Al_mGa_{1-m}N$/GaN interface given as

$$|\sigma(m)| = |P_{\rm sp}(Al_mGa_{1-m}N) - P_{\rm sp}(GaN) + P_{\rm pz}(Al_mGa_{1-m}N)| \tag{3}$$

with $P_{\rm sp}$ as the spontaneous polarization of AlGaN and GaN [24], [25], [38].

The piezoelectric polarization ($P_{\rm pz}$) depends on the strain generated at the $Al_mGa_{1-m}N$/GaN interface to accommodate the difference in lattice constants of GaN and AlGaN. For a FS device, piezoelectric polarization induced charge density is given as

$$P_{\rm pz}(Al_mGa_{1-m}N) = 2\left(\frac{a(0)-a(m)}{a(m)}\right)\left(e_{31}(m) - e_{33}(m)\frac{C_{13}(m)}{C_{33}(m)}\right), \quad \text{for } 0\le m\le 1 \tag{4}$$

where $a(m)$ is the lattice constant, $e_{31}(m)$ and $e_{33}(m)$ are piezoelectric constants, and $C_{13}(m)$ and $C_{33}(m)$ are elastic constants [38], [39].

However, for a given thickness of the $Al_mGa_{1-m}N$ barrier layer, increasing the aluminum content increases lattice mismatch, which, in turn, results in lattice relaxation with strain reduction. For a PR device with an $Al_mGa_{1-m}N$ layer thickness in range of 200–400 Å, piezoelectric polarization induced charge density depends on the Al mole fraction as [31]

$$P_{\rm pz}(Al_mGa_{1-m}N) = \begin{cases} 2\left(\dfrac{a(0)-a(m)}{a(m)}\right)\left(e_{31}(m)-e_{33}(m)\dfrac{C_{13}(m)}{C_{33}(m)}\right), \\ \quad \text{for } 0 \le m < 0.38 \\ 2\dfrac{(2.33-3.5m)}{\left(\dfrac{a(m)}{a(0)-a(m)}\right)}\left(e_{31}(m)-e_{33}(m)\dfrac{C_{13}(m)}{C_{33}(m)}\right), \\ \quad \text{for } 0.38 \le m \le 0.67 \\ 0, \qquad \text{for } 0.67 < m \le 1. \end{cases} \tag{5}$$

Equation (5) shows that the device remains completely strained for Al content up to 38% and fully relaxed for Al content greater than 67%. It is actually in the range from 38% to 67% that the device is PR with $((3.5m-1.33)\times 100)\%$ relaxation.

### A. Current–Voltage Characteristics

The drain current ($I_{\rm ds}$) is obtained from current density equation as

$$I_{\rm ds}(m,x) = Wq\mu(x)\left(n_s(m,x)\frac{dV_c(x)}{dx} + \frac{k_BT}{q}\frac{dn_s(m,x)}{dx}\right) \tag{6}$$

where $W$ is the gatewidth, $k_B$ is the Boltzmann constant, $T$ is the temperature, and $\mu(x)$ is the field-dependent electron mobility given [35] and [40] as

$$\mu(x) = \frac{\mu_o}{1+\left(\dfrac{\mu_oE_c-v_{\rm sat}}{E_cv_{\rm sat}}\right)\dfrac{dV_c(x)}{dx}} \tag{7}$$

where $\mu_o$ is the low-field mobility, $E_c$ is the critical electric field, and $v_{\rm sat}$ is the saturation drift velocity of the electron. Using (1) and (7) in (6), we obtain

$$I_{\rm ds}(m,x)\left(1+\left(\frac{\mu_oE_c-v_{\rm sat}}{E_cv_{\rm sat}}\right)\frac{dV_c(x)}{dx}\right) = \frac{W\mu_o\varepsilon(m)}{(d_d+d_i+\Delta d)}\left(V'_{\rm gs}(m)-V_c(x)\right)\frac{dV_c(x)}{dx} \tag{8}$$

where

$$V'_{\rm gs}(m) = V_{\rm gs}-V_{\rm th}(m)-\frac{k_BT}{q}.$$

Integrating (8) with boundary conditions

$$V_c(x)|_{x=0} = I_{\rm ds}(m)R_s \tag{9a}$$

and

$$V_c(x)|_{x=L} = V_{\rm ds}-I_{\rm ds}(m)(R_s+R_d) \tag{9b}$$

where $L$ is the gate length, $V_{\rm ds}$ is the applied drain bias, and $R_s$ and $R_d$ are the parasitic source and drain resistance, respectively, the $I_{\rm ds}$–$V_{\rm ds}$ equation for the linear region is obtained as

$$I_{\rm ds}(m) = \frac{-A_2(m)+\sqrt{A_2(m)^2-4A_1(m)A_3(m)}}{2A_1(m)} \tag{10}$$

with

$$A_1(m) = \left(\frac{\mu_oE_c-v_{\rm sat}}{E_cv_{\rm sat}}\right)(2R_s+R_d) - \left(\frac{W\mu_o\varepsilon(m)}{2(d_d+d_i+\Delta d)}\right)\left(R_d^2+2R_sR_d\right)$$

$$A_2(m) = \left(\frac{W\mu_o\varepsilon(m)}{d_d+d_i+\Delta d}\right) \cdot \left(V_{\rm ds}(R_s+R_d)-V'_{\rm gs}(m)(2R_s+R_d)\right) - L - V_{\rm ds}\left(\frac{\mu_oE_c-v_{\rm sat}}{E_cv_{\rm sat}}\right)$$

$$A_3(m) = \left(\frac{W\mu_o\varepsilon(m)}{d_d+d_i+\Delta d}\right)\left(V'_{\rm gs}(m)V_{\rm ds}-\frac{V_{\rm ds}^2}{2}\right).$$

Substituting (1) in (6) and assuming that the carrier mobility, electric field, and channel potential attain the values $\mu_o$, $E_c$, and $V_{d\rm sat}(m)$, respectively, at the onset of saturation, the drain saturation current is obtained as

$$I_{d\rm sat}(m) = \frac{W\varepsilon(m)\mu_oE_c}{(d_d+d_i+\Delta d)}\left(V'_{\rm gs}(m)-V_{d\rm sat}(m)\right) \tag{11}$$

where $V_{d\rm sat}(m)$ is the drain saturation voltage obtained by equating $I_{d\rm sat}(m)$ with $I_{\rm ds}(m)|_{V_{\rm ds}=V_{d\rm sat}(m)}$ and is given as

$$V_{d\rm sat}(m) = \frac{-B_2(m)-\sqrt{B_2(m)^2-4B_1(m)B_3(m)}}{2B_1(m)} \tag{12}$$

where

$$B_1(m) = \gamma(m)+\left(\frac{W\mu_o\varepsilon(m)}{d_d+d_i+\Delta d}\right)\left(\left(\frac{\mu_oE_c-v_{\rm sat}}{v_{\rm sat}}\right)-\frac{1}{2}\right) - \left(\frac{W\mu_o\varepsilon(m)}{d_d+d_i+\Delta d}\right)^2E_c(R_s+R_d)$$

$$\gamma(m) = \left(\frac{W\mu_o\varepsilon(m)E_c}{d_d+d_i+\Delta d}\right)^2\left(\frac{\mu_oE_c-v_{\rm sat}}{E_cv_{\rm sat}}\right)(2R_s+R_d) - \left(\frac{W\mu_o\varepsilon(m)}{d_d+d_i+\Delta d}\right)^3\frac{E_c^2}{2}\left(R_d^2+2R_sR_d\right)$$

$$B_2(m) = \left(\frac{W\mu_o\varepsilon(m)}{d_d+d_i+\Delta d}\right)\left(\frac{\mu_oE_cV'_{\rm gs}(m)}{v_{\rm sat}}+E_cL\right) - 2V'_{\rm gs}(m)\gamma(m)+\left(\frac{W\mu_o\varepsilon(m)}{d_d+d_i+\Delta d}\right)^2 \cdot E_cV'_{\rm gs}(m)(3R_s+2R_d)$$

$$B_3(m) = \gamma(m)V'_{\rm gs}(m)^2-\left(\frac{W\mu_o\varepsilon(m)}{d_d+d_i+\Delta d}\right)V'_{\rm gs}(m)LE_c - \left(\frac{W\mu_o\varepsilon(m)}{d_d+d_i+\Delta d}\right)^2V'_{\rm gs}(m)^2E_c(2R_s+R_d).$$

### B. Small-Signal Parameters

The small-signal parameters—drain conductance, transconductance, cutoff frequency, and transit time—govern the current-driving capability and are extremely important for estimating the microwave performance of a device. The small-signal parameters have been modeled in terms of basic device parameters and terminal voltages to give an insight into device performance and serve as a basis for device design and optimization.

*1) Drain/Output Conductance:* The drain conductance is an important microwave parameter that determines the maximum voltage gain attainable from a device. The drain conductance of the $Al_mGa_{1-m}N$/GaN HEMT is evaluated as

$$g_d(m) = \left.\frac{\partial I_{\rm ds}(m)}{\partial V_{\rm ds}}\right|_{V_{\rm gs}}. \tag{13}$$

Using (10) in (13), we obtain

$$\begin{aligned} g_d(m) = \frac{1}{2A_1(m)} &\left(\left(\frac{W\mu_o\varepsilon(m)}{d_d+d_i+\Delta d}\right)(R_s+R_d)\right. \\ &\left.-\left(\frac{\mu_o E_c - v_{\rm sat}}{E_c v_{\rm sat}}\right)\right) \\ &\cdot\left(\frac{A_2(m)}{\sqrt{A_2(m)^2-4A_1(m)A_3(m)}}-1\right) \\ &-\left(\frac{W\mu_o\varepsilon(m)}{d_d+d_i+\Delta d}\right)\left(\frac{V'_{\rm gs}(m)-V_{\rm ds}}{\sqrt{A_2(m)^2-4A_1(m)A_3(m)}}\right). \end{aligned} \tag{14}$$

*2) Transconductance:* The transconductance is the most important parameter for optimization of FET high-frequency behavior. The major part of the gain mechanism is embodied in the active channel transconductance, which is evaluated as

$$g_m(m) = \left.\frac{\partial I_{\rm ds}(m)}{\partial V_{\rm gs}}\right|_{V_{\rm ds}}. \tag{15}$$

Using (10) in (15), we obtain the transconductance in the linear region $g_{m\rm lin}(m)$ as

$$\begin{aligned} g_{m\rm lin}(m) = &\left(\frac{W\mu_o\varepsilon(m)}{d_d+d_i+\Delta d}\right) \\ &\cdot\left(\frac{2R_s+R_d}{2A_1(m)}\left(1-A_2(m)\right)\right. \\ &\left.-\frac{V_{\rm ds}}{\sqrt{A_2(m)^2-4A_1(m)A_3(m)}}\right). \end{aligned} \tag{16}$$

The transconductance in the saturation region $g_{m\rm sat}(m)$ is obtained by substituting (11) in (15) and is given as

$$g_{m\rm sat}(m) = \left(\frac{W\mu_o\varepsilon(m)E_c}{d_d+d_i+\Delta d}\right)\left(1-\alpha(m)\right) \tag{17}$$

where

$$\begin{aligned} \alpha(m) = &\left(\frac{-1}{2B_1(m)}\right)\left(1+\frac{B_2(m)}{\sqrt{B_2(m)^2-4B_1(m)B_3(m)}}\right) \\ &\cdot\beta_1(m)+\frac{1}{\sqrt{B_2(m)^2-4B_1(m)B_3(m)}}\,\beta_2(m) \end{aligned}$$

with

$$\begin{aligned} \beta_1(m) = &\left(\frac{W\mu_o\varepsilon(m)}{d_d+d_i+\Delta d}\right)\left(\frac{\mu_o E_c}{v_{\rm sat}}\right)-2\gamma(m) \\ &+\left(\frac{W\mu_o\varepsilon(m)}{d_d+d_i+\Delta d}\right)^2 E_c(3R_s+2R_d) \\ \beta_2(m) = &\,2\gamma(m)V'_{\rm gs}(m)-LE_c\left(\frac{W\mu_o\varepsilon(m)}{d_d+d_i+\Delta d}\right) \\ &-2E_cV'_{\rm gs}(m)(2R_s+R_d)\left(\frac{W\mu_o\varepsilon(m)}{d_d+d_i+\Delta d}\right)^2. \end{aligned}$$

*3) Cutoff Frequency:* The primary figure-of-merit for high-frequency performance of a device is the current-gain cutoff frequency. The cutoff frequency of the AlGaN/GaN HEMT is calculated as

$$f_t(m) = \frac{g_m(m)(d_d+d_i+\Delta d)}{2\pi WL\varepsilon(m)} \tag{18}$$

where the maximum constant value of gate capacitance is assumed, as the region under the gate is fully depleted under normal operating conditions.

*4) Transit Time:* The transit-time effect is the result of a finite time being required for carriers to traverse from source to drain. Smaller transit times are desirable to attain a high-frequency response from a device. The transit time for the $Al_mGa_{1-m}N$/GaN HEMTs is evaluated as

$$\tau_t(m) = \frac{1}{2\pi f_t(m)}. \tag{19}$$

## III. Results and Discussion

Fig. 2 shows the variation of the 2-DEG sheet charge density with an Al mole fraction ($m$) of $Al_mGa_{1-m}N$ barrier layer for FS and PR $Al_mGa_{1-m}N$/GaN HEMTs. This figure shows that high sheet charge density of approximately $6.89\times10^{12}$ cm$^{-2}$ is obtained at $m = 0.2$ in the absence of doping, which is attributed to the presence of strong spontaneous and piezoelectric polarization fields. An increase in doping ($N_d$) of the $Al_mGa_{1-m}N$ barrier results in higher values of 2-DEG density. However, in actual practice, the maximum value of $N_d$ that can be used to increase the 2-DEG density is limited by the presence of donor defects, barrier traps, and surface traps, which lead to increased scattering and reduced conduction. The 2-DEG density increases with an increase in the Al mole fraction of the barrier, owing to the increase in conduction-band discontinuity and polarization-induced charges. This figure shows that 2-DEG density in a PR structure is much less than that expected for an FS device at the same Al mole fraction. For $d = 200$ Å and $N_d = 3.5\times10^{18}$ cm$^{-3}$, the 2-DEG sheet charge density at $m = 0.5$ is $2.01\times10^{13}$ cm$^{-2}$ for a PR device, while it would rise to $2.45\times10^{13}$ cm$^{-2}$ if the device is assumed to remain unrelaxed or FS. Results for the undoped and doped devices are in good agreement with the experimental results [31]. The results indicate that the maximum 2-DEG density that can be attained in an $Al_mGa_{1-m}N$/GaN HEMT

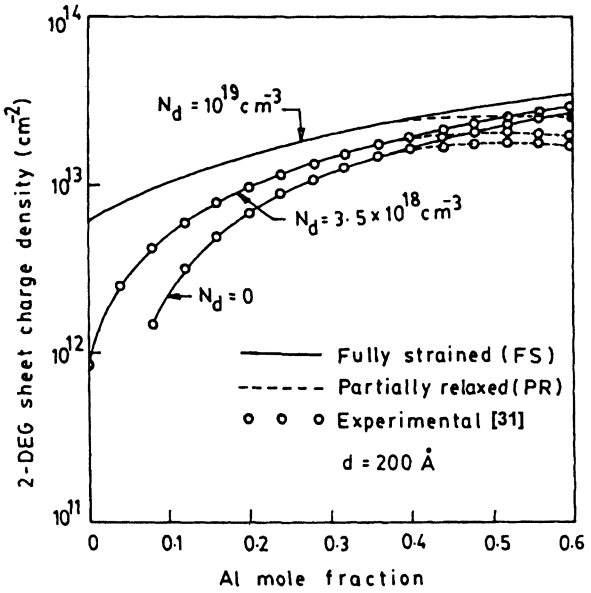


Fig. 2. Variation of 2-DEG density with the Al mole fraction of the $Al_mGa_{1-m}N$ barrier layer for various values of doping density.

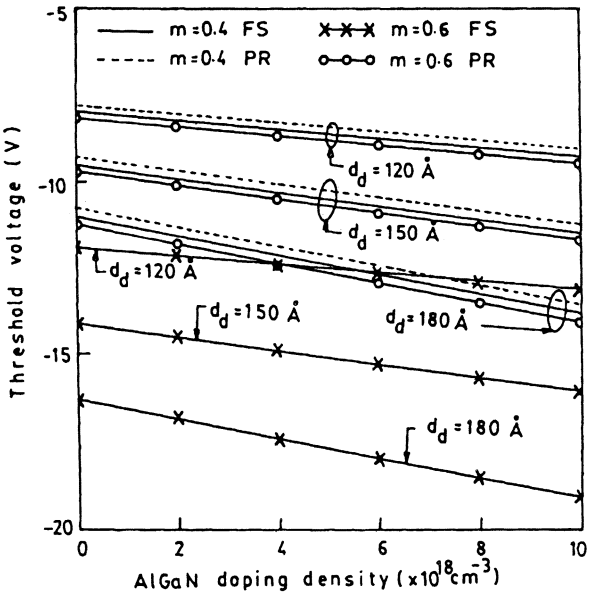


Fig. 3. Variation of threshold voltage of $Al_mGa_{1-m}N$/GaN HEMT with a doping density of the $Al_mGa_{1-m}N$ barrier for various values of barrier thickness and Al mole fractions with and without the effect of strain relaxation.

depends more strongly on strain relaxation of the barrier than on the Al content. Thus, an analysis of both fully and partially strained structures is essential to accurately estimate the 2-DEG density of the high Al-content $Al_mGa_{1-m}N$/GaN HEMT.

The variation of threshold voltage ($V_{\rm th}$) with doping concentration, thickness ($d_d$), and aluminum content ($m$) of the $Al_mGa_{1-m}N$ barrier is shown in Fig. 3. The threshold voltage decreases to more negative values with an increase in doping and thickness of the barrier, with the decrease being more dominant for higher thickness. This figure shows that for $m = 0.4$, $V_{\rm th}$ decreases from $-8.05$ to $-11.3$ V at $N_d = 2 \times 10^{18}$ cm$^{-3}$ and from $-8.81$ to $-12.91$ V at $N_d = 8 \times 10^{18}$ cm$^{-3}$, as the doped layer thickness is increased from 120 to 180 Å. This is because a higher reverse bias is needed to deplete a higher density of electrons located at a larger effective distance from the gate. An increase in the Al content of the $Al_mGa_{1-m}N$ layer also leads to a decrease in the threshold voltage due to the corresponding increase in the polarization induced charge density. It is clear from the figure that if the device is assumed to be FS, $V_{\rm th}$ shows a drastic fall at higher Al mole fractions. However, for a PR device, the effect is much less pronounced. For $d_d = 120$ Å and $N_d = 4 \times 10^{18}$ cm$^{-3}$, the threshold voltage shifts from $-8.51$ to $-8.3$ V at $m = 0.4$, while it shifts to a much larger extent from $-14.88$ to $-8.67$ V for $m = 0.6$ when the effect of relaxation is incorporated. This clearly shows that threshold voltage would be largely overestimated if the strain relaxation of the barrier is not considered at higher Al mole fractions. With an increase in doping density of the AlGaN barrier, the threshold voltage further decreases to values that may not be achievable in realistic devices. This is due to the fact that, in actual device operation, the pinchoff characteristics are governed by the gate leakage currents, which are highly undesirable for microwave applications. The off-state leakage current is predominantly due to vertical tunneling of electrons from the metal gate through the semiconductor [42]. Low doping and higher Schottky barrier height are desired to attain nonleaky gates to obtain good pinchoff characteristics. The figure shows that $V_{\rm th}$ of $-10$ V can be attained with 150-Å-thick barrier at doping densities of $1.92 \times 10^{18}$ cm$^{-3}$ and $2.89 \times 10^{18}$ cm$^{-3}$ for $m = 0.6$ and 0.4, respectively. Thus, the first device ($N_d = 1.92 \times 10^{18}$ cm$^{-3}$ and $m = 0.6$) would be a better choice to reduce the leakage currents. Further, a GaN cap layer is usually fabricated on top of the standard barrier layer that suppresses vertical tunneling and reduces gate leakage to a large extent.

Fig. 4(a) and (b) shows the current voltage characteristics of PR $Al_mGa_{1-m}N$/GaN HEMTs with Al mole fractions of 0.4, 0.5, and 0.6. The drain current increases with an increase in aluminum content of the $Al_mGa_{1-m}N$ layer owing to the increase in 2-DEG density, consistent with high mobility. Although the low-temperature mobility decreases with increasing Al content, which may be due to enhanced interface scattering or remote alloy scattering, the room temperature mobility remains nearly unaffected [27]. As shown in Fig. 4(a), the drain current for the PR device increases from 4.41 to 4.72 A/mm at $V_{\rm gs} = -2$ V as the Al mole fraction increases from 0.4 to 0.6. However, in case the device is assumed to be FS, the current would be expected to rise from 4.6 A/mm at $m = 0.4$ to 8.12 A/mm at $m = 0.6$. The results show a drastic reduction of current by 3.4 A/mm for $m = 0.6$, as compared to a decrease of only 0.19 A/mm for $m = 0.4$, the difference being due to relaxation of only 7% at $m = 0.4$ as compared to that of 77% at $m = 0.6$. The results for the PR $Al_{0.4}Ga_{0.6}N$/GaN HEMT are in close agreement with previously published simulated results [41]. Fig. 4(b) shows the current voltage characteristics of the $Al_{0.5}Ga_{0.5}N$/GaN HEMT with a gate length of 0.7 $\mu$m for various values of gate voltages. If the device is assumed to be FS at $m = 0.5$, the maximum drain current at $V_{\rm gs} = 2$ V is expected to be 1786.7 mA/mm. However, stain relaxation of the AlGaN barrier (degree of relaxation being 42% at $m = 0.5$) results in a much smaller drain current of 1100.4 mA/mm at the same gate bias. The results

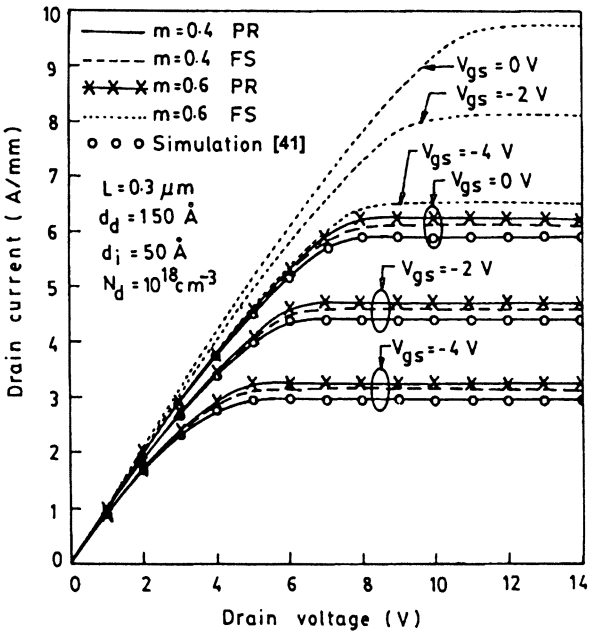


(a)

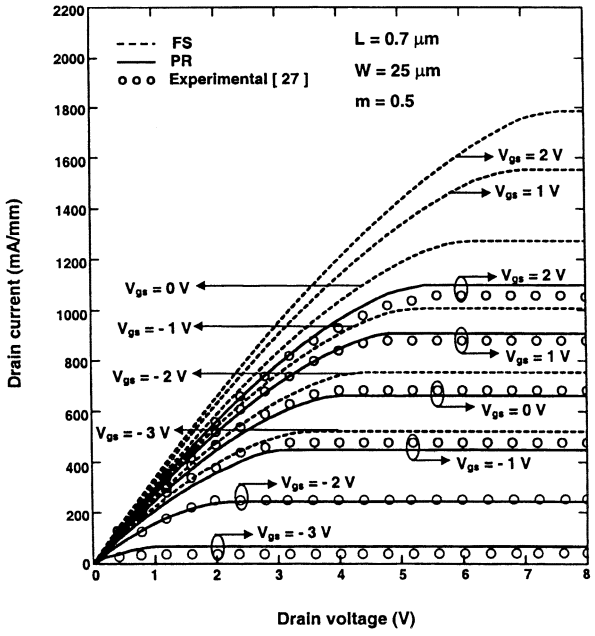


(b)

Fig. 4. (a) Current–voltage characteristics of the FS and PR $Al_mGa_{1-m}N$/GaN HEMT for $m = 0.4$ and $m = 0.6$. (b) Current–voltage characteristics of the FS and PR $Al_mGa_{1-m}N$/GaN HEMT for $m = 0.5$.

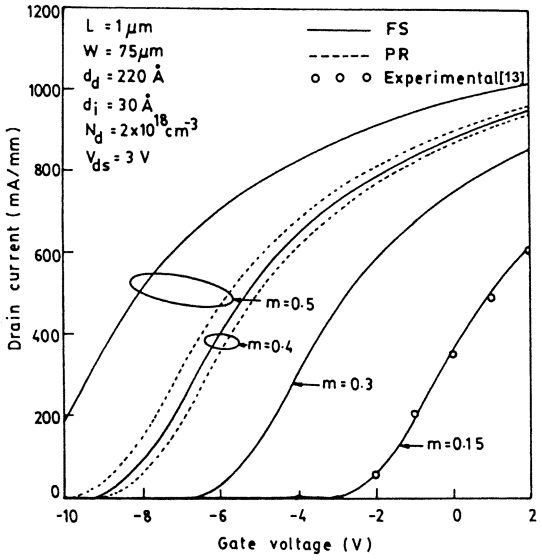


(a)

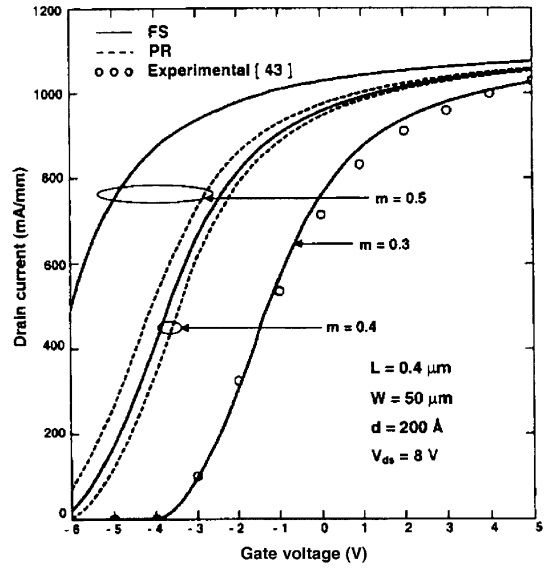


(b)

Fig. 5. (a) Dependence of drain current on gate voltage for the FS and PR 1-$\mu$m gate-length $Al_mGa_{1-m}N$/GaN HEMT at different Al contents. (b) Dependence of drain current on gate voltage for the FS and PR 0.4-$\mu$m gate-length $Al_mGa_{1-m}N$/GaN HEMT at different Al contents.

predicted for the PR device compare well with previously published experimental results [27].

Fig. 5(a) and (b) shows the dependence of the drain current on gate voltage for fully and partially strained devices with different aluminum mole fraction for two different sets of device parameters. GaN-based HEMTs exhibit very high current density owing to the unique material properties that enable improved charge confinement and carrier transport. As the reverse gate bias is increased, the depth of potential well at the heterointerface decreases, resulting in reduced 2-DEG density and reduced current. The drain current increases appreciably with an increase in aluminum content; the increase being more dominant at lower gate voltages. Fig. 5(a) shows a drain current of 787.05 and 769.69 mA/mm at a gate bias of $-2$ V for FS and PR devices, respectively, with $m = 0.4$. With an increase in mole fraction to 0.5, the current at $V_{gs}$ of $-2$ V increases to 911.26 and 811.47 mA/mm for FS and PR devices respectively. Thus, for PR devices, the increase in current with Al mole fraction is much less than in FS devices. The threshold voltage also shifts to more negative values as the Al mole fraction increases. The results for the FS $Al_{0.15}Ga_{0.85}N$/GaN HEMT are in good agreement with published experimental data [13]. Fig. 5(b) shows that as the aluminum content of the 0.4-$\mu$m gate-length $Al_mGa_{1-m}N$/GaN HEMT is increased from 0.3 to 0.5, the drain current for the FS device is expected to increase from 567.9 to 1010.1 mA/mm at $V_{gs} = -1$ V. However, strain

relaxation of the AlGaN barrier layer at $m = 0.5$ results in a smaller drain current of 930.6 mA/mm at $V_{gs} = -1$ V. The predicted results for the FS $Al_{0.3}Ga_{0.7}N$/GaN HEMT compare well with previously published experimental results [43].

Fig. 6(a) and (b) shows the variation of transconductance ($g_m$) with gate voltage for various PR and FS device structures. As the Al mole fraction of the $Al_mGa_{1-m}N$ barrier layer is increased, the peak transconductance shows a large shift toward negative gate voltages; the shift being larger for higher mole fractions. Thus, at higher mole fractions, peak transconductance can be attained at much lower values of gate bias. The peak $g_m$ occurs at the gate voltage that just begins to cause some noticeable occupation of ionized donors under the gate. At a lower bias, $g_m$ is degraded by the resistive drop through the channel and, at a higher bias, it is degraded because the gate charge fills the AlGaN donors rather than the channel with electrons. High values of transconductance in GaN-based HEMTs are attributed to high peak and saturation velocities and high carrier density due to strong polarization effects. Fig. 6(a) shows that the gate voltage corresponding to the peak transconductance decreases from $-1$ V at $m = 0.15$ to $-4.5$ V at $m = 0.3$ and from $-7$ V at $m = 0.4$ to $-9.75$ V at $m = 0.5$ for FS devices. However, for $m$ larger than 0.38, the device becomes PR due to elastic strain relaxation of the barrier and peak transconductance occurs at gate voltages of $-6.75$ and $-7.75$ V, respectively, for $m = 0.4$ and 0.5. The shift in gate voltage corresponding to the peak transconductance, due to relaxation, is $-2$ V at $m = 0.5$, as compared to the shift of only $-0.25$ V for $m = 0.4$. This is due to the fact that the degree of relaxation increases from 7% to 42%, as the Al mole fraction is increased from 0.4 to 0.5. Fig. 6(b) shows the $g_m$–$V_{gs}$ characteristics for a different device structure. For aluminum concentration of 50%, a peak of $g_m$ is attained at gate voltages of $-8.2$ and $-5.8$ V for FS and PR devices, respectively, whereas for 40% aluminum content, the corresponding peaks occur at gate voltages of $-5.4$ and $-5.0$ V, respectively. The predicted results for the FS device with an Al mole fraction of 0.3 and a gate length of 0.4 $\mu$m are in good agreement with published experimental data [43]. Thus, it is extremely essential to account for strain relaxation of the $Al_mGa_{1-m}N$ barrier to accurately determine the small-signal characteristics of high Al-content $Al_mGa_{1-m}N$/GaN HEMTs. In Fig. 6, the authors could not compare their predicted results for higher mole fractions (>0.3) due to the nonavailability of published experimental/simulated data. Only the results for $m = 0.15$ ($L = 1$ $\mu$m) and $m = 0.3$ ($L = 0.4$ $\mu$m) are compared and are found to be in close agreement with the published results of dc measurements [13], [43].

Fig. 7 shows the variation of output/drain conductance of $Al_mGa_{1-m}N$/GaN HEMTs with drain voltage for PR and FS devices with different Al mole fractions. The drain conductance increases with an increase in the Al mole fraction and decreases with an increase in drain voltage. For $m = 0.5$, the drain conductance in FS and PR devices is obtained as 0.66 and 0.44 S/mm, respectively, at $V_{gs} = -2$ V and $V_{ds} = 6$ V. The inset of Fig. 7 shows the dependence of the drain conductance on the gate voltage at a drain bias of 4 V for devices with various Al mole fractions. The drain conductance increases

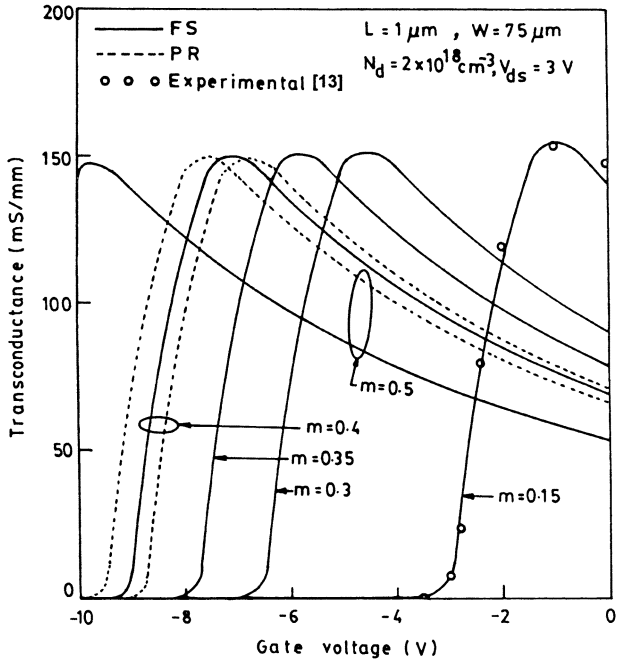


(a)

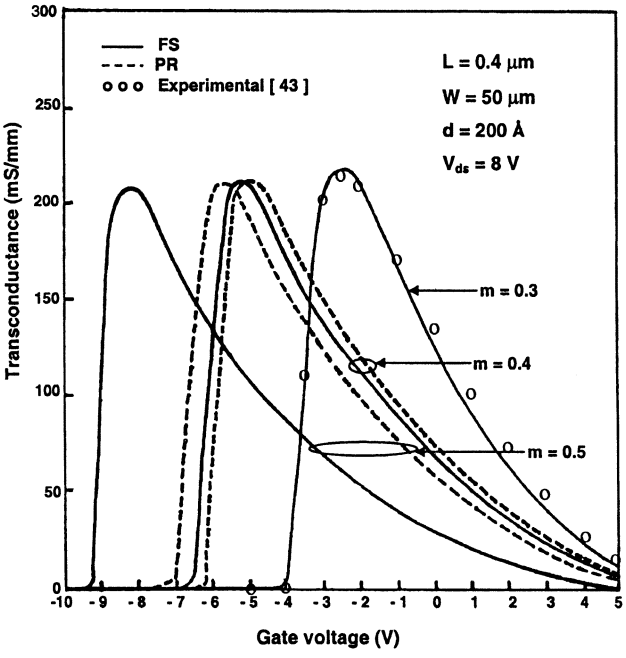


(b)

Fig. 6. (a) Variation of transconductance with gate voltage for various values of Al mole fractions of the $Al_mGa_{1-m}N$ barrier for the 1-$\mu$m gate-length $Al_mGa_{1-m}N$/GaN HEMT. (b) Variation of transconductance with gate voltage for various values of Al mole fractions of the $Al_mGa_{1-m}N$ barrier for 0.4-$\mu$m gate-length $Al_mGa_{1-m}N$/GaN HEMT.

with an increase in the Al content, the increase being more dominant at lower gate voltages. The authors could not compare their predicted results of drain conductance due to the nonavailability of published experimental/simulated data. The drain conductance model has been derived from the current–voltage formulation, which has been compared with published results [41], as shown in Fig. 4(a).

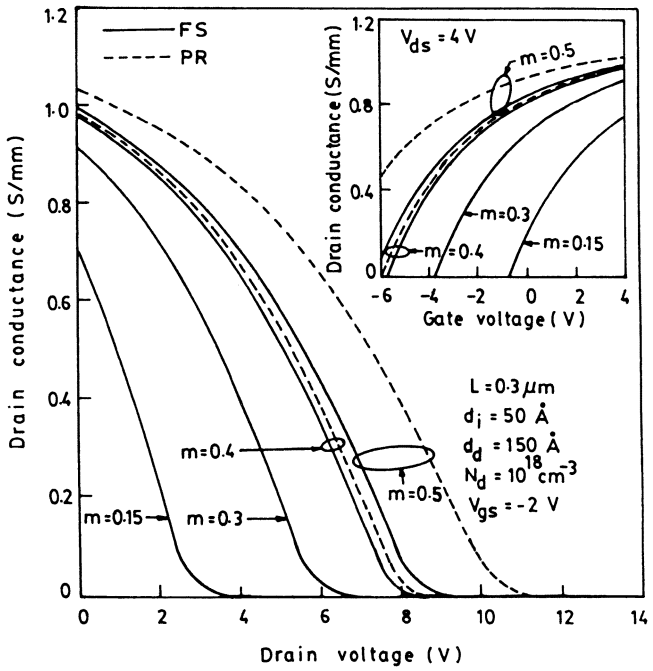


Fig. 7. Dependence of drain conductance on drain voltage at $V_{\rm gs} = -2$ V for various Al mole fractions with and without relaxation. (*inset*) Variation of drain conductance with gate voltage for various Al mole fractions at a drain bias of 4 V.

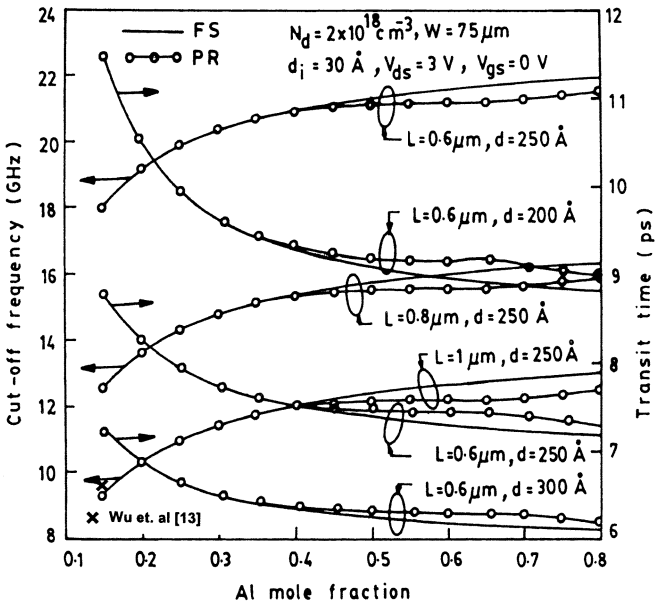


Fig. 8. Variation of current-gain cutoff frequency and transit time with an Al mole fraction of the $Al_mGa_{1-m}N$ barrier for various values of gate length and barrier thickness.

Fig. 8 shows the variation of current gain cutoff frequency and transit time of the $Al_mGa_{1-m}N$/GaN HEMT with an Al mole fraction for various values of gate length and $Al_mGa_{1-m}N$ layer thickness. The transit time decreases with the increasing aluminum content and thickness of the $Al_mGa_{1-m}N$ barrier layer. The cutoff frequency and transit time of FS ($m \leq 0.38$), PR ($0.38 \leq m \leq 0.67$) and fully relaxed ($m \geq 0.67$) $Al_mGa_{1-m}N$/GaN HEMTs have been analyzed for different gate lengths as a function of the Al mole fraction ($m$). At $L = 1$ $\mu$m and $d = 250$ Å, the cutoff frequency of the device with $m = 0.15$ (FS) is predicted to be 9.4 GHz, which is in close agreement with the published experimental results [13]. Results of cutoff frequency and transit time for higher mole fractions were not compared due to the nonavailability of published data. The cutoff frequency increases with a decrease in gate length and with an increase in Al content, but at mole fractions above 0.38, strain relaxation of the barrier leads to smaller frequencies for PR structures, as compared to the FS device. The $Al_{0.6}Ga_{0.4}N$/GaN HEMT exhibits high frequency of 21.18 GHz at a gate length of 0.6 $\mu$m, which translates into a cutoff frequency gate-length ($f_t$–$L_g$) product of 12.7 GHz $\cdot$ $\mu$m. The effective electron velocity ($v_{\rm eff}$) under the gate is estimated from the dependence of cutoff frequency on gate length

$$\left(f_t = \left(\frac{v_{\rm eff}}{2\pi L_g}\right)\right)$$

and is obtained as 8.17 cm $s^{-1}$. It is observed that $f_t$ in $Al_mGa_{1-m}N$/GaN HEMTs is much smaller than in other conventional/pseudomorphic HEMTs. However, the superiority of GaN-based HEMTs lies in the fact that power applications (for which $Al_mGa_{1-m}N$/GaN HEMTs are basically used) require the RF figures-of-merit to remain high at very large drain voltages. The cutoff frequency of conventional devices collapses drastically at increased drain voltages because of drain delay in the extended depletion region. However, in $Al_mGa_{1-m}N$/GaN system, $f_t$ maintains a value, within 80% of its peak value over a very wide range of drain voltages [44]. This is possibly due to greater high-field electron velocity in GaN. The $f_t$–$L_g$ product can be improved by doping the GaN channel, which results in higher 2-DEG densities and reduced parasitic series resistance. A larger effective mass of electrons in GaN makes the electron mobility less sensitive to channel doping, especially at higher temperatures. Doped channel devices with an $f_t$–$L_g$ product larger than 18 GHz $\cdot$ $\mu$m have been demonstrated [45].

Fig. 9 shows the variation of transit time ($\tau_t$) of the FS and PR AlGaN/GaN HEMT with gate voltage. Minimum transit time is attained at the gate voltage that corresponds to the peak transconductance, thus indicating that $g_m$ determines the ultimate speed of a switching device. As the gate voltage approaches the threshold, $\tau_t$ increases drastically as the channel begins to pinch off and there is no current flow. Also, transit time increases with an increase in gate voltage to more positive values due to the resulting transconductance degradation. As AlGaN has lower mobility and electron velocity, as compared to the normal GaN channel, the device conductance is degraded with higher transit times and lower device speed. Fig. 9 also shows the effect of Al composition on transit time variation with gate voltage. Increase in Al content shifts the gate voltage corresponding to a minimum $\tau_t$ to more negative values.

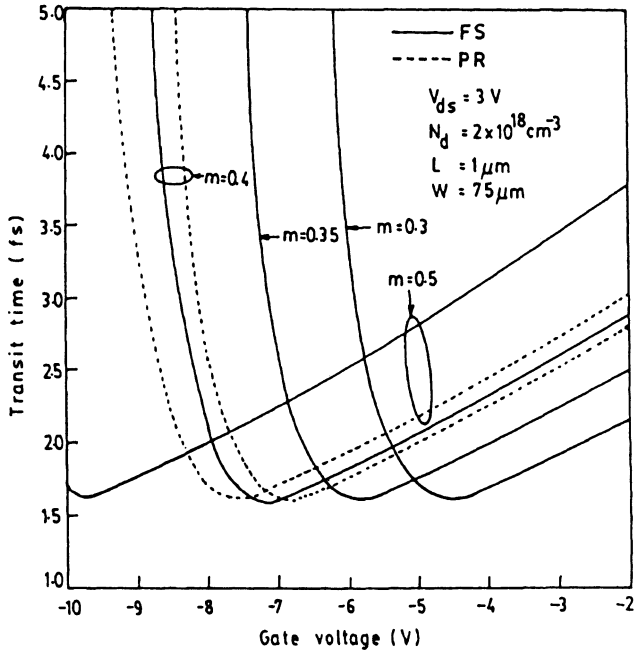


Fig. 9. Variation of transit time of the FS and PR $Al_mGa_{1-m}N$/GaN HEMT with gate voltage for various values of Al mole fractions.

## IV. Conclusion

An accurate model has been developed to predict the current–voltage characteristics, drain conductance, transconductance, cutoff frequency, and transit time of FS and PR lattice-mismatched $Al_mGa_{1-m}N$/GaN HEMTs. The main emphasis of the analysis is a relative comparison of different $Al_mGa_{1-m}N$/GaN HEMTs with varied mole fractions to analyze the feasibility of FS, PR, and fully relaxed devices for microwave applications. Results indicate that the dependence of spontaneous and piezoelectric polarization on alloy composition is extremely crucial in determining the performance of GaN-based HEMTs, particularly in high Al-content devices. The utilization of higher Al content to attain higher 2-DEG densities and improved microwave performance requires gauging of the elastic strain along with other device parameters. Strain relaxation of the barrier at higher Al mole fractions imposes an upper limit on the maximum 2-DEG density and necessitates the analysis of PR $Al_mGa_{1-m}N$/GaN HEMTs to assess the microwave performance of AlGaN/GaN HEMTs. For an AlGaN/GaN HEMT, the maximum channel current is set by the conduction-band discontinuity between the AlGaN barrier layer and GaN channel layer. Device optimization and performance has to do with increasing the discontinuity by increasing the mole fraction. However, achieving high crystal quality, decreased trapping centers, and low resistance ohmic contacts are the main technological challenges that need to be addressed for optimum overall performance of high Al-content GaN-based HEMTs that would be extremely useful for high-power microwave applications.

## References

[1] S. N. Mohammad, A. A. Salvador, and H. Morkoc, "Emerging gallium nitride based devices," *Proc. IEEE*, vol. 83, pp. 1306–1355, Oct. 1995.

[2] M. N. Yoder, "Gallium nitride: Past, present and future," in *Int. Electron Devices Meeting Technical Dig.*, 1997, pp. 3–12.

[3] M. S. Shur, "GaN based transistors for high power applications," *Solid State Electron.*, vol. 42, no. 12, pp. 2131–2138, 1998.

[4] U. K. Mishra, Y. F. Wu, B. P. Keller, S. Keller, and S. P. Denbaars, "GaN based microwave power HEMTs," in *Proc. Int. Physics of Semiconductor Devices Workshop*, 1998, pp. 878–883.

[5] J. C. Zolper, "Wide bandgap semiconductor microwave technologies: From promise to practice," in *Int. Electron Devices Meeting Technical Dig.*, 1999, pp. 389–392.

[6] ——, "Progress toward ultra-wideband AlGaN/GaN MMICs," *Solid State Electron.*, vol. 43, pp. 1479–1482, 1999.

[7] R. S. Gupta, Rashmi, A. Kranti, and S. Haldar, "Modeling of $Al_xGa_{1-x}N$/GaN heterostructure field effect transistors (HFET's) for microwave and millimeter wave applications," in *11th Int. Physics of Semiconductor Devices Workshop*, vol. 2, New Delhi, India, 2001, pp. 819–826.

[8] Y. Ohno and M. Kuzuhara, "Application of GaN-based heterojunction FETs for advanced wireless communication," *IEEE Trans. Electron Devices*, vol. 48, pp. 517–523, Mar. 2001.

[9] S. Strite and H. Morkoc, "GaN, AlN and InN: A review," *J. Vac. Sci. Technol. B, Microelectron. Process. Phenom.*, vol. 10, no. 4, pp. 1237–1266, 1992.

[10] O. Ambacher, "Growth and applications of group III-nitrides," *J. Phys. D, Appl. Phys.*, vol. 31, no. 20, pp. 2653–2710, 1998.

[11] S. J. Pearton, J. C. Zolper, R. J. Shul, and F. Ren, "GaN: Processing, defects and devices," *J. Appl. Phys.*, vol. 86, no. 1, pp. 1–78, 1999.

[12] Rashmi, S. Haldar, and R. S. Gupta, "An analytical 2-dimensional model for AlGaN/GaN modulation doped field effect transistor (MODFET)," in *Advances in Electronics Symp.*, Varanasi, India, 2001, pp. 123–127.

[13] Y. F. Wu, S. Keller, P. Kozodoy, B. P. Keller, P. Parikh, D. Kapolnek, S. P. Denbaars, and U. K. Mishra, "Bias dependent microwave performance of AlGaN/GaN MODFET's up to 100 V," *IEEE Electron Device Lett.*, vol. 18, pp. 290–292, June 1997.

[14] N. Maeda, T. Nishida, N. Kobayashi, and M. Tomizawa, "Two-dimensional electron-gas density in $Al_xGa_{1-x}N$/GaN heterostructure field-effect transistor," *Appl. Phys. Lett.*, vol. 73, no. 13, pp. 1856–1858, 1998.

[15] R. Li, S. J. Cai, L. Wong, Y. Chen, K. L. Wang, R. P. Smith, S. C. Martin, K. S. Boutros, and J. M. Redwing, "An $Al_{0.3}Ga_{0.7}N$/GaN undoped channel heterostructure field effect transistor with $f_{max}$ of 107 GHz," *IEEE Electron Device Lett.*, vol. 20, pp. 323–325, July 1999.

[16] N. Q. Zhang, S. Keller, G. Parish, S. Heikman, S. P. Denbaars, and U. K. Mishra, "High breakdown GaN HEMT with overlapping gate structure," *IEEE Electron Device Lett.*, vol. 21, pp. 373–375, Sept. 2000.

[17] Y. F. Wu, D. Kapolnek, J. P. Ibbetson, P. Parikh, B. P. Keller, and U. K. Mishra, "Very high power density AlGaN/GaN HEMTs," *IEEE Trans. Electron Devices*, vol. 48, pp. 586–590, Mar. 2001.

[18] W. Lu, J. Yang, M. A. Khan, and I. Adesida, "AlGaN/GaN HEMTs on SiC with over 100 GHz $f_t$ and low microwave noise," *IEEE Trans. Electron Devices*, vol. 48, pp. 581–585, Mar. 2001.

[19] P. M. Asbeck, E. T. Yu, S. S. Lau, G. J. Sullivan, J. Van Hove, and J. Redwing, "Piezoelectric charge densities in AlGaN/GaN HFETs," *Electron. Lett.*, vol. 33, no. 14, pp. 1230–1231, 1997.

[20] E. T. Yu, G. J. Sullivan, P. M. Asbeck, C. D. Wang, D. Qiao, and S. S. Lau, "Measurement of piezoelectrically induced charge in GaN/AlGaN heterostructure field effect transistor," *Appl. Phys. Lett.*, vol. 71, no. 19, pp. 2794–2796, 1997.

[21] H. Morkoc, R. Cingolani, and B. Gil, "Polarization effects in nitride semiconductor device structures and performance of modulation doped field effect transistors," *Solid State Electron.*, vol. 43, pp. 1753–1771, 1999.

[22] Rashmi, A. Kranti, S. Haldar, and R. S. Gupta, "A physics based charge control model of lattice mismatched AlGaN/GaN HEMTs," in *11th Int. Physics of Semiconductor Devices Workshop*, vol. 2, New Delhi, India, 2001, pp. 911–914.

[23] A. Bykhovski, B. Gelmont, and M. Shur, "The influence of the strain-induced electric field on the charge distribution in GaN–AlN–GaN structure," *J. Appl. Phys.*, vol. 74, no. 11, pp. 6734–6739, 1993.

[24] E. S. Hellman, "The polarity of GaN: A critical review," *MRS Internet J. Nitride Semiconduct. Res. 3*, vol. 11, pp. 1–11, 1998.

[25] O. Ambacher, J. Smart, J. R. Shealy, N. G. Weimann, K. Chu, M. Murphy, W. J. Schaff, L. F. Eastman, R. Dimitrov, L. Wittmer, M. Stutzmann, W. Rieger, and J. Hilsenbeck, "Two-dimensional electron gases induced by spontaneous and piezoelectric polarization charges in N- and Ga-face AlGaN/GaN heterostructures," *J. Appl. Phys.*, vol. 85, no. 6, pp. 3222–3233, 1999.

[26] Y. F. Wu, B. P. Keller, P. Fini, J. Pusl, M. Le, N. X. Nguyen, C. Nguyen, D. Widman, S. Keller, S. P. Denbaars, and U. K. Mishra, "Short channel $Al_{0.5}Ga_{0.5}N$/GaN MODFET's with power density >3 W/mm at 18 GHz," *Electron. Lett.*, vol. 33, no. 20, pp. 1742–1743, 1997.

[27] Y. F. Wu, B. P. Keller, P. Fini, S. Keller, T. J. Jenkins, L. T. Kehias, S. P. Denbaars, and U. K. Mishra, "High Al-content AlGaN/GaN MODFET's for ultrahigh performance," *IEEE Electron Device Lett.*, vol. 19, pp. 50–53, Feb. 1998.

[28] Y. F. Wu, D. Kapolnek, J. Ibbetson, N. Q. Zhang, P. Parikh, B. P. Keller, and U. K. Mishra, "High Al-content AlGaN/GaN HEMT's on SiC substrates with very high power performance," in *Int. Electron Devices Meeting Technical Dig.*, 1999, pp. 925–927.

[29] Y. Zhang and J. Singh, "Charge control and mobility studies for an AlGaN/GaN high electron mobility transistor," *J. Appl. Phys.*, vol. 85, no. 1, pp. 587–594, 1999.

[30] A. D. Bykhovski, B. L. Gelmont, and M. S. Shur, "Elastic strain relaxation and piezoeffect in GaN–AlN, GaN–AlGaN and GaN–InGaN superlattices," *J. Appl. Phys.*, vol. 81, no. 9, pp. 6332–6338, 1997.

[31] O. Ambacher, B. Foutz, J. Smart, J. R. Shealy, N. G. Weimann, K. Chu, M. Murphy, A. J. Sierakowski, W. J. Schaff, L. F. Eastman, R. Dimitrov, A. Mitchell, and M. Stutzmann, "Two-dimensional electron gases induced by spontaneous and piezoelectric polarization in undoped and doped AlGaN/ GaN heterostructures," *J. Appl. Phys.*, vol. 87, no. 1, pp. 334–344, 2000.

[32] S. Terao, M. Iwaya, R. Nakamura, S. Kamiyama, H. Amano, and I. Akasaki, "Fracture of $Al_xGa_{1-x}N$/GaN heterostructure: Compositional and impurity dependence," *Jpn. J. Appl. Phys.*, vol. 40, pp. L195–L197, 2001.

[33] B. Shen, T. Someya, and Y. Arakawa, "Influence of strain relaxation of the $Al_xGa_{1-x}N$ barrier on transport properties of the two-dimensional electron gas in modulation doped $Al_xGa_{1-x}N$/GaN heterostructures," *Appl. Phys. Lett.*, vol. 76, no. 19, pp. 2746–2748, 2000.

[34] S. Wu, R. T. Webster, and A. F. M. Anwar, "Physics-based intrinsic model for AlGaN/GaN HEMTs," *MRS Internet J. Nitride Semiconduct. Res., 4S1, G 6.58*, 1999.

[35] P. P. Ruden, J. D. Albrecht, A. Sutandi, S. C. Binari, K. Ikossi-Anastasiou, M. G. Ancona, R. L. Henry, D. D. Koleske, and A. E. Wickenden, "Extrinsic performance limitations of AlGaN/GaN heterostructure field effect transistors," *MRS Internet J. Nitride Semiconduct. Res., 4S1, G 6.35*, 1999.

[36] Rashmi, A. Agarwal, S. Sen, S. Haldar, and R. S. Gupta, "Analytical model for DC characteristics and small signal parameters of AlGaN/GaN modulation doped field effect transistors for microwave circuit applications," *Microwave Opt. Technol. Lett.*, vol. 27, pp. 413–418, 2000.

[37] Rashmi, S. Haldar, and R. S. Gupta, "2-D analytical model for current voltage characteristics and output conductance of AlGaN/GaN MODFET," *Microwave Opt. Technol. Lett.*, vol. 29, pp. 117–123, 2001.

[38] Y. Zhang, I. P. Smorchkova, C. R. Elsass, S. Keller, J. P. Ibbetson, S. Denbaars, U. K. Mishra, and J. Singh, "Charge control and mobility in AlGaN/GaN transistors: Experimental and theoretical studies," *J. Appl. Phys.*, vol. 87, no. 11, pp. 7981–7987, 2000.

[39] T. Li, R. P. Joshi, and C. Fazi, "Monte Carlo evaluations of degeneracy and interface roughness effects on electron transport in AlGaN–GaN heterostructures," *J. Appl. Phys.*, vol. 88, no. 2, pp. 829–837, 2000.

[40] Rashmi, A. Kranti, S. Haldar, and R. S. Gupta, "An accurate charge control model for spontaneous and piezoelectric polarization dependent two-dimensional electron gas (2-DEG) sheet charge density of lattice mismatched AlGaN/GaN HEMTs," *Solid State Electron.*, vol. 46, no. 5, pp. 621–630, 2002.

[41] F. Sacconi, A. DiCarlo, P. Lugli, and H. Morkoc, "Spontaneous and piezoelectric polarization effects on the output characteristics of AlGaN/GaN heterojunction modulation doped FETs," *IEEE Trans. Electron Devices*, vol. 48, pp. 450–457, Mar. 2001.

[42] E. J. Miller, X. Z. Dang, and E. T. Yu, "Gate leakage current mechanisms in AlGaN/GaN heterostructure field-effect transistors," *J. Appl. Phys.*, vol. 88, no. 10, pp. 5951–5958, 2000.

[43] S. C. Binari, K. Ikossi, J. A. Roussos, W. Kruppa, D. Park, H. B. Dietrich, D. D. Koleske, A. E. Wickenden, and R. L. Henry, "Trapping effects and microwave power performance in AlGaN/GaN HEMTs," *IEEE Trans. Electron Devices*, vol. 48, pp. 465–471, Mar. 2001.

[44] Y. F. Wu, B. P. Keller, S. Keller, N. X. Nguyen, M. Le, C. Nguyen, T. J. Jenkins, L. T. Kehias, S. P. Denbaars, and U. K. Mishra, "Short channel AlGaN/GaN MODFET's with 50 GHz $f_t$ and 1.7 W/mm output power at 10 GHz," *IEEE Electron Device Lett.*, vol. 18, pp. 438–440, 1997.

[45] M. A. Khan, Q. Chen, J. W. Yang, M. S. Shur, B. T. Dermott, and J. A. Higgins, "Microwave operation of GaN/AlGaN-doped channel heterostructure field effect transistors," *IEEE Electron Devices Lett.*, vol. 17, pp. 325–327, July 1996.

**Rashmi** was born in New Delhi, India, in 1977. She received the B.Sc. (with honors) and M.Sc. degrees in physics from St. Stephen's College, University of Delhi, Delhi, India, in 1997 and 1999, respectively, and the Ph.D. degree in electronics science from the University of Delhi, in 2002.

Her research interests include semiconductor device physics and technology, modeling of GaN-based high-power HEMTs for microwave applications, and novel device structures for analog applications.

**Abhinav Kranti** was born in New Delhi, India in 1975. He received the B.Sc. (with honors) and M.Sc. degrees in physics from St. Stephen's College, University of Delhi, Delhi, in 1996 and 1998, respectively, and the Ph.D. degree in electronic science from the University of Delhi, in 2001.

He is currently a Post-Doctoral Research Fellow with the Electromagnetic Microwave and Communications (EMIC) Laboratory, Université Catholique de Louvain (UCL), Louvain-la-Neuve, Belgium. His research interests include semiconductor device physics, process and device modeling, novel FET structures for advanced CMOS applications, and GaN-based wide-bandgap semiconductors for millimeter and microwave applications.

Dr. Kranti was the recipient of the Outstanding Student Paper submitted to the 2001 IEEE Topical Meeting on Silicon Monolithic Integrated Systems in RF Systems.

**Subhasis Haldar** was born in India, in 1967. He received the B.Sc. (with honors) and M.Sc. degrees in physics and the Ph.D. degree in electronics from the University of Delhi, India, in 1988, 1990, and 1995, respectively.

In 1991, he joined the Semiconductor Device Research Laboratory, Department of Electronic Science, University of Delhi, where he developed analytical models for both MOSFET and MESFET devices. In 1993, he joined the Motilal Nehru College, University of Delhi, as a Lecturer, and is currently a Reader. His current field of interest is miniaturization of devices, study and suppression of hot carrier effect considering lightly doped drain (LDD) and fully overlapped lightly doped drain (FOLD) structures, single- and double-gate MOSFETs, surrounding gate/cylindrical devices, and Polysilicon thin-film transistors (TFTs). He has authored or coauthored approximately 95 technical papers published in journals and conference proceedings.

Dr. Haldar was member of the International Symposium on Recent Advances in Microwave Technology (ISRAMT'93) and joint secretary of the Asia–Pacific Microwave Conference (APMC'96). He is the joint secretary of the Asia–Pacific Microwave Conference (APMC'04), New Delhi, India.

**Mridula Gupta** (M'00) received the B.Sc. degree in physics, M.Sc. degree in electronics, M.Tech. degree in microwave electronics, and Ph.D. degree in optoelectronics from the University of Delhi, Delhi, India, in 1984, 1986, 1988, and 1998, respectively.

In 1989, she joined the Department of Electronic Science, University of Delhi, as a Lecturer and is currently a Reader. She has authored or coauthored approximately 45 publications in international and national journals and conferences. Her current research interests include modeling and simulation of MOSFETs, MESFETs, and HEMTs for microwave-frequency applications.

She is a Fellow of the Institution of Electronics and Telecommunication Engineers, India and Life Member of the Semiconductor Society of India. She is a secretary of the Asia–Pacific Microwave Conference (APMC'04), New Delhi, India.

**R. S. Gupta** (SM'81) received the B.Sc. and M.Sc. degrees from Agra University, Agra, India, in 1963 and 1966, respectively, and the Ph.D. degree in electronic engineering from the Institute of Technology, Banaras Hindu University, Varanasi, India, in 1970.

In 1971, he joined Ramjas College, University of Delhi, Delhi, India. In 1987, he joined the Department of Electronic Science, University of Delhi, where he is currently a Professor. His current interests and activities cover modeling of SOI submicrometer MOSFETs and LDD MOSFETs, modeling and design of HEMTs, hot-carrier effects in MOSFETs and modeling of GaAs MESFETs for high-performance microwave and millimeter-wave circuits, and quantum-effect devices. In 1988, he was a Visitor with the University of Sheffield, Sheffield, U.K., under the ALIS Link Exchange Program. In 1995, he visited several U.S. universities and several universities in Spain in 1999. He has authored or coauthored over 250 papers in various international and national journals and conferences. He heads several major research projects sponsored by the Ministry of Defense, Department of Science and Technology, Council of Science, and Industrial Research and University Grants Commission. He has generated 22 Ph.D. students and currently has ten doctoral students working under him. He is listed in *Who's Who in the World*.

Prof. Gupta is a Fellow of the Institution of Electronics and Telecommunication Engineers, India, Life Member of the Indian Chapter of the International Centre for Theoretical Physics (ICTP), and Life Member of the Semiconductor Society of India. He is currently an executive member of the IEEE Electron Devices (ED)/Microwave Theory and Techniques (MTT) chapter India Council. He was the secretary of both the International Symposium on Recent Advances in Microwave Technology (ISRAMT'93) and the Asia–Pacific Microwave Conference (APMC'96) and the chairman of the Technical Program Committee of APMC'96. He also edited the proceedings for both of these international conferences. He is a chairman of the Asia–Pacific Microwave Conference (APMC'04), New Delhi, India. His name has appeared in the Golden List of the IEEE TRANSACTIONS ON ELECTRON DEVICES.